# 霊長類における循環器疾患モデルの紹介

揚山直英
医薬基盤研究所霊長類医科学研究センター

## Ⅰ. はじめに

霊長類医科学研究センターはカニクイザルの大規模繁殖コロニーを30年以上にわたり維持しているという，世界でも類を見ない施設である．そのためコロニー内には様々な自然発生疾患モデルが存在することが明らかとなりつつあり，さらに特殊施設や設備を生かした様々な疾患モデルを用いた研究も幅広く展開されている．著者らはこれまでそれらのモデルを用いた様々な研究に従事してきたが，最近では新規治療法などの開発研究が最も急がれる循環器疾患に着目している．本稿では，そのような霊長類循環器疾患モデルを紹介するとともに，そうしたモデルを用いた応用研究についても言及したい．

## Ⅱ. 背景および目的

循環器疾患は世界各国で死亡原因の上位にあげられ，問題となっていることから，その新規治療・診断・予防法の樹立が求められている．そのエビデンス獲得のためには，モデル動物が必須であるというのはいうまでもない事実でもある．さらに，昨今では循環器疾患をはじめとした様々な疾患に対する研究を発展させるために，前臨床研究も含めてヒトに最も近縁な霊長類，すなわちサル類のモデルが必須となりつつあり，その需要が高まっている．しかしながら一方で，サル類の循環器疾患の報告自体がほとんどなく，また，その検査や評価方法すらも確立されていないということがわかってきた．すなわち，循環器疾患の研究を展開する以前に，サル類の客観的な評価系が必要であるということになる．そこでわれわれは，サル類における診断技術の確立や，高感度検出系，体系的調査など，評価系の樹立や疾患モデルの樹立を試みた．

## Ⅲ. 方　　法

サル類における循環器疾患研究を可能とすべく，その基盤となる技術として画像診断や電気生理学的な評価系の構築を進めた．例えば，ヒト新生児相当の小さなサル類に適応したレントゲン造影やMRI装置などの特殊設備を導入し，特化した画像診断方法の樹立を成し遂げた．また，心エコーもプローブの選定，周波数帯域の適応，装置の構築などに工夫を凝らし，サルの特徴に合わせた機器の改善や測定方法の樹立を図った．それらに加え心電図，テレメトリー・ホルター心電計，HRV解析などといった電気生理学的な評価手法の確立も行った．特にそれらのなかで，後述する心磁計については新たな診断技術のひとつとしての可能性も秘めていることから，注目を集めている．これらの設備，技術を駆使してカニクイザル繁殖コロニーの大規模スクリーニングや様々な循環器疾患の評価，抽出，作出を行った．その後，それら評価手法や技術を用いたスクリーニングデータより種々の大規模データベースを構築した．例えば，心エコーから算出される指標のひとつである左心室短縮率と心室内径などからは，サルの正常範囲が得られると同時に，そこから逸脱する個体は心機能が低下し，心室内径が拡張するなど拡張型心筋症様の病態を示していることがわかり，疾患の抽出に役立てることが可能となった．また，心電図からもQTcなどの重要な指標が得られ，毒性，安全性試験に有用な不整脈の評価基準のひとつとしても役立てられた．さらに，MRIや心磁計

からもデータベースやイメージング評価基準を得ることが可能であった．こうした基準を利用しスクリーニングを行うことで，サル繁殖コロニー内に多様な自然発生の循環器疾患が存在する事実がわかってきた．それらのなかにはサル類では初の報告となる心室中隔欠損や弁膜症，右室二腔症などの貴重な症例も含まれている[1]．本稿では，これらの疾患のなかから自然発生の心筋症や不整脈疾患，さらに実験的誘発心筋梗塞モデルなどを中心に紹介する．

## Ⅳ．拡張型心筋症モデル

心筋症には肥大型，拘束型などのいくつかの分類があり，そのなかのひとつに拡張型心筋症がある．病態もいくつかの形態を示すが，拡張相を呈すなどして最終的には主に心不全をきたす．重症化すると，対症療法としては基本的に心臓移植などの外科的治療しかなく，根治療法はほぼないともいえる．そのため，難治性疾患に分類され，その新規治療法や予防法の開発研究が重点的に進められている疾患のひとつでもある．今回，本研究成果によって，その疾患の唯一のモデルとなりうる可能性を示す霊長類モデルが抽出された．まず，その所見としては心電図で左室高電位差を示し，レントゲン所見でも明らかな心胸郭比の拡大を認めた．さらに心エコーでも左室の拡張と機能低下が認められた．また，MRIでも壁運動の異常，造影による心筋バイアビリティの低下が見て取れた．これらの病態は，ヒトの病態を忠実に反映していることもわかっている．その後，治療を施したにもかかわらず重度な病態を呈して死亡した個体の病理組織学的検索を行ったところ，拡張型心筋症に特有の病理所見も示した(図1)．

以上より，カニクイザル繁殖コロニーにおいて重度の心不全症状を呈し，ヒト病態を模倣する拡張型心筋症個体が存在することが明らかとなり，貴重な疾患モデルとしての樹立が示唆された．心筋症や心不全の病態機序はいまだわかっていないことが多い．本疾患モデルを用いてその解明を進めることは，心臓病態学の発展ならびに本疾患の新規治療・

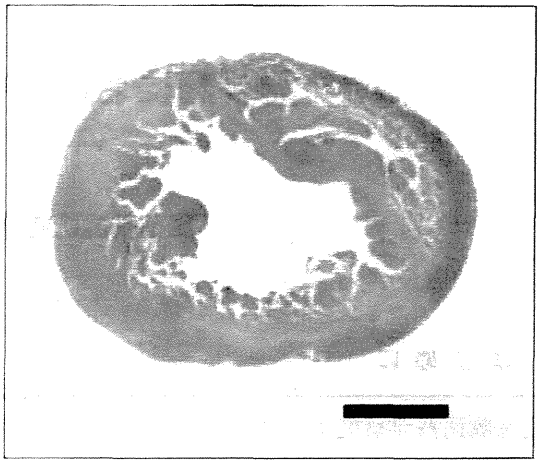

**図1　拡張型心筋症個体の心臓病理標本**
心筋間質のびまん性線維化(青)，心筋の錯綜交差配列や脱落および菲薄化などが認められる(マッソントリクローム染色，Bar=10 mm)．

診断法開発研究に多くの知見を与えるものと思われる．現在，本モデルを利用して，Mutationや疾患関連タンパク質の解析，心疾患の新たなバイオマーカーの可能性をもつ物質の解析やイメージングなどのアプローチも進めており，その成果が期待されている．

## Ⅴ．不整脈モデル：非接触磁気計測手法に基づく電気生理学的評価

非接触磁気計測手法とは心臓の電気生理学的機能を検査する新たな手法であり，新たな不整脈疾患などの診断方法になる可能性を秘めている．心臓では，心筋細胞内の電気興奮に伴うイオン電流によって，微弱な磁場が発生することがわかっている．この心臓から発生する微弱な磁場を超伝導粒子干渉素子により測定し，心磁図というイメージングデータとして評価を可能にする装置が心磁計である．その心磁計の特長としては，生体内の透磁率が一定の微弱磁場を高感度に測定できることから，高い空間分解能をもち，電気生理的活動を三次元的に測定でき多点計測が可能であること，さらに，非侵襲かつ非接触で測定できることなどがあげられる．これまでのところ，ヒトでの研究を通して，この心磁図が虚血性心疾患・不整脈・胎児心疾患の早期診断に有効

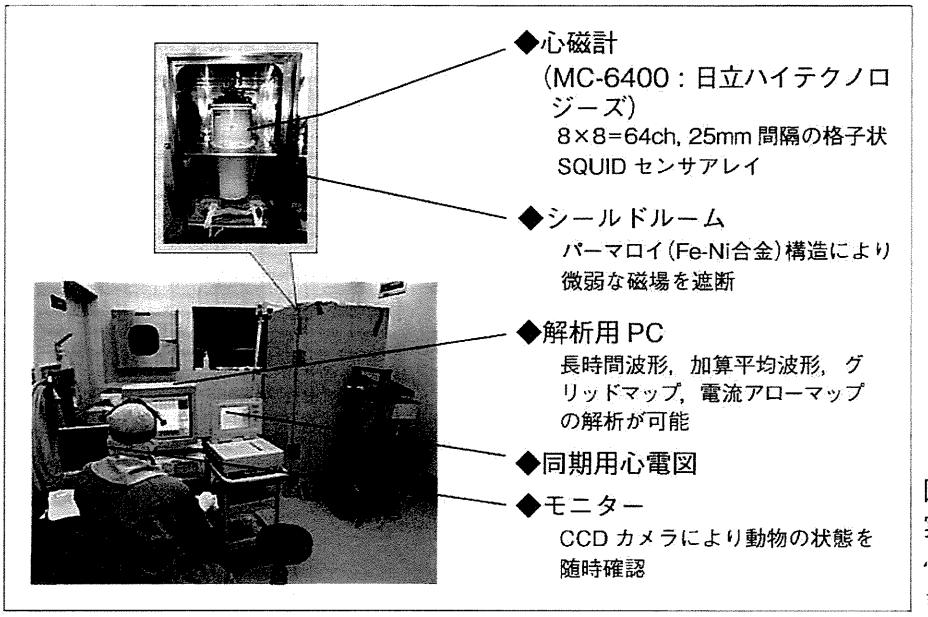


図2
実験システム
心磁計を用いた非接触磁気計測の実験システムおよび測定風景.

表1　測定したカニクイザルのデータ

| | | Females n=51 | Males n=44 | Total n=95 |
|---|---|---|---|---|
| Age (years) | Mean±SD | 19.3±8.7 | 11.2±8.6 | 15.6±9.5 |
| | Range | 1.2～34.8 | 1.8～33.8 | 1.2～34.8 |
| Weight (kg) | Mean±SD | 3.6±1.0 | 5.1±1.5 | 4.3±1.5 |
| | Range | 1.3～6.1 | 2.5～9.6 | 1.3～9.6 |

であることが報告されている.

サル類に特化した実験システムとして，64 chの心磁計(日立ハイテクノロジーズ製)をシールドルームやモニタリング装置，同期用心電図などと組み合わせて構築した(図2)．このシステムによりサルを心磁計の下に数分寝かせるだけで，安全に，非侵襲的，非接触でデータを採取することが可能となった．これらのシステムを用い，主にカニクイザルを対象として非接触磁気計測を施行した.

表1に示したように，これまで1歳から34歳までの動物(雄44頭，雌51頭)の測定を行った．さらに，これらの個体はすべて心電図の同期下で測定を行い，同時に心エコー，レントゲン，血液検査などの循環器専門検査も行い，その病態を診断した.

本測定からは，図3に示した長時間心磁波形や加算平均波形が最初に得られ，これらには心電図波形同様の診断概念が適応できることが明らかとなっている．次いでグリッドマップといわれる画像では，心臓の多点での電気生理学的な情報を得ることが可能となる．これらサルから得られた波形を正常なヒトのものと比較したところ，磁場強度や周期はその大きさの違いからヒトの半分程度になるものの，形としてはほぼ同様の相似形を有する波形を得られることがわかった．したがって，ヒト新生児相当の大きさのカニクイザルにおいても心臓磁場が適切に測定できることが明らかとなった[2].

引き続き，前述の健常ザルから得られたデータより解析用プログラムを通して，電流アローマップを作成した(図4)．その結果，サルのP波成分では心房の興奮は右房から左房が遅れ，QRS波形では左

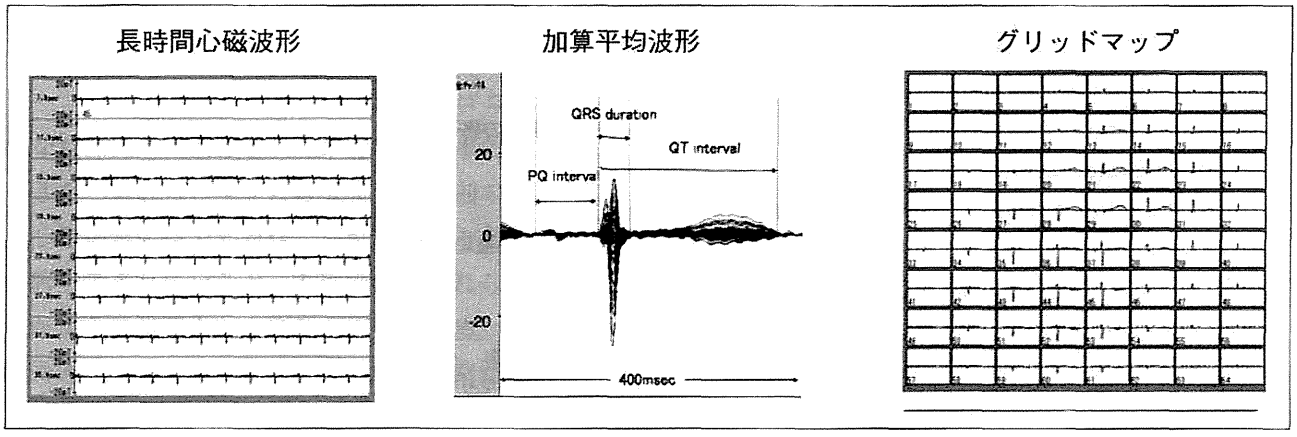


図３　カニクイザルの各種心磁図

心電図，心エコー，レントゲン検査で異常は認められず健康体と診断された６歳，３kgのメスのカニクイザルから得られた正常心磁波形．

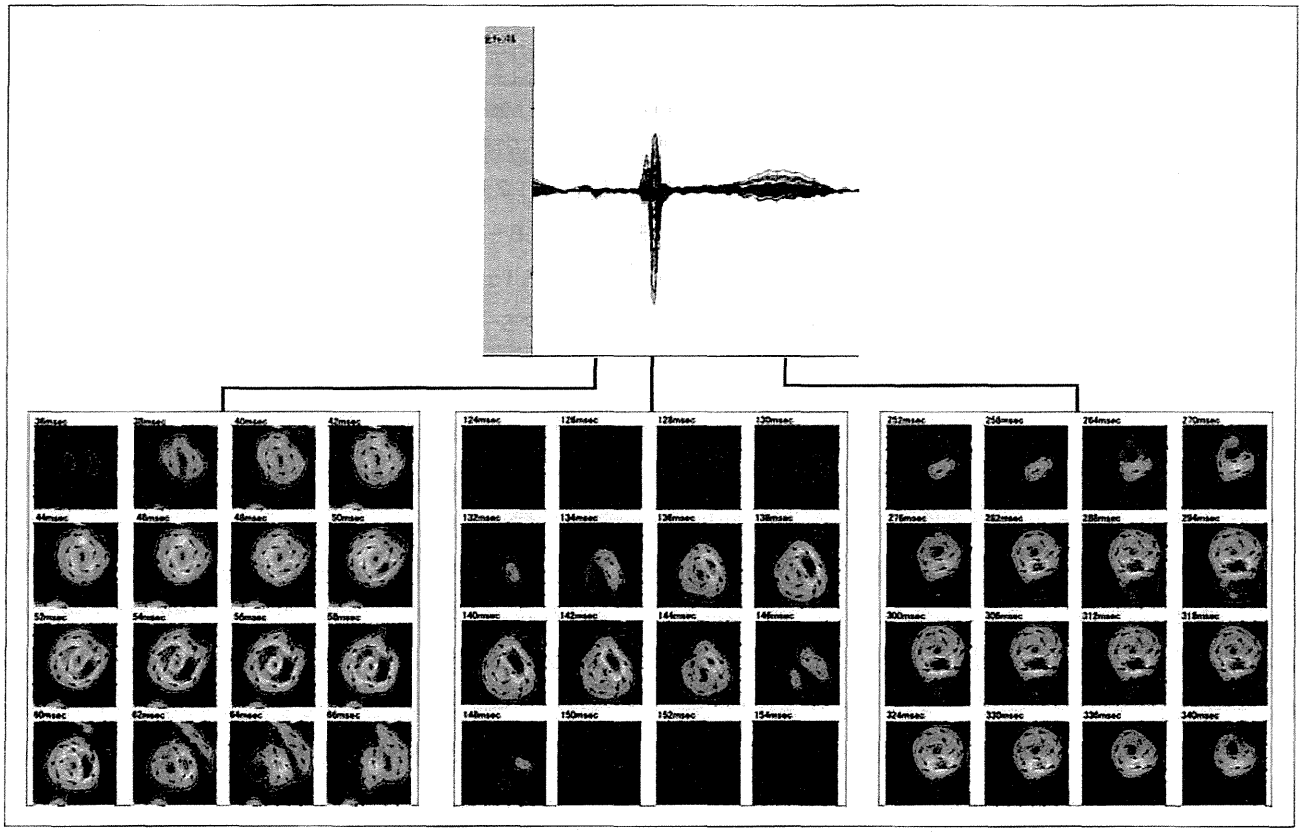

図４　健常ザルの電流アローマップ

グリッドマップを重ね合わせた波形から，単位時間あたりで心臓の各部位の電気的活動をイメージングとして評価できる電流アローマップが得られる．

表２　心磁図の加算平均波形から得られたPQ間隔，QRS振幅，QT間隔とQTcの各数値

| | | Females n=51 | Males n=44 | Total n=95 |
|---|---|---|---|---|
| PQ interval | Means±SD | 77±13 | 80±14 | 79±14 |
| | Range | 52～108 | 48～111 | 48～111 |
| QRS duration | Means±SD | 41±6 | 44±7 | 42±7 |
| | Range | 31～58 | 30～63 | 30～63 |
| QT interval | Means±SD | 220±26 | 225±21 | 225±23 |
| | Range | 171～283 | 187～264 | 171～283 |
| QTc | Means±SD | 365±29 | 361±20 | 363±25 |
| | Range | 286～432 | 316～395 | 286～432 |

表３　心磁図より得られたカニクイザルの各種疾患分類

| | Females n=51 | Males n=44 | Total n=95 |
|---|---|---|---|
| Normal | 23 | 12 | 35 |
| Bundle branch block | 1 | 4 | 5 |
| Brugada syndrome | 1 | 4 | 5 |
| WPW syndrome | 0 | 3 | 3 |
| LQT syndrome | 5 | 1 | 6 |
| Cardiomyopathy | 4 | 9 | 13 |
| Unknown | 17 | 11 | 28 |

右の脚から心室全体に興奮が伝わり，T波における心室の再分極では興奮は同一方向にのみ伝達する画像が認められた(図４)．これらはヒトの所見とほぼ一致したものであり，ヒト新生児相当の大きさの霊長類からも正常な電流アローマップが記録可能であることが示唆された．

表２に心磁図から得られた各パラメーターの数値を示した．各数値は雌雄間でいずれも有意差は認められなかったものの，これらの数値は心電図から得られた各種パラメーターともほぼ相同する値となり，長年培われた心電図の概念もそのまま応用できることが明らかとなった．以上より，サル類における心磁図の評価基準が世界で初めて樹立されたこととなる[3]．

さらに，それら評価基準との詳細な比較によって表３に示したようなWPW症候群，QT延長症候群，脚ブロック，Brugada症候群などの所見を示す個体を見いだすことができた[4]．現在，これら疾患の精査，確定診断を試みており，不整脈疾患の新規治療診断方法などに有用なモデルとして樹立することを検討している．

このように，高感度，高解像度のイメージング手法である新規診断法としての可能性を秘めた心磁計をサル類に適応したことで，その組み合わせ自体が様々な創薬，治療の安全性・有効性評価に適したシステムとして樹立されることが期待されている．

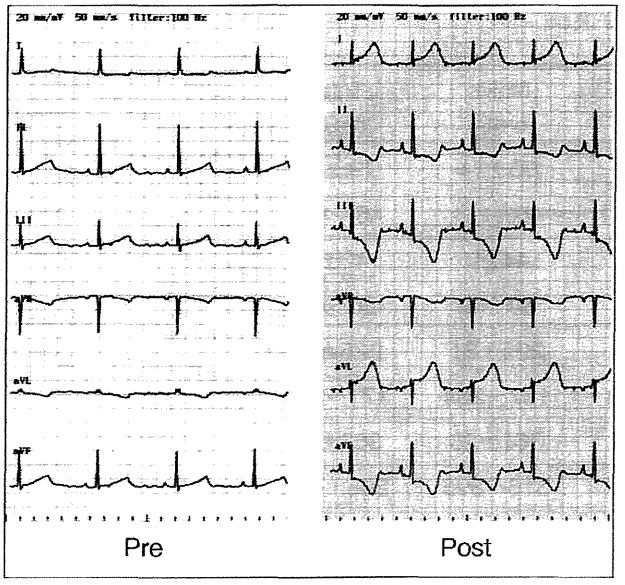


図５　心電図所見
梗塞直後からST上昇が認められ，心筋梗塞の特徴的な所見を示した．

## Ⅵ．心筋梗塞モデル

現在，心筋梗塞は我が国の死亡原因のなかでも癌に次いで数が多く，治療法もカテーテル手術やバイパス手術など多くの手法が存在する．しかしながら，重篤で多様な病態を示す疾患であり，患者数も増大していることから，さらなる早期診断や予後判定法の開発研究が常に求められている．そのため，ヒト病態を忠実に再現し，慢性病態をも評価することが可能なサルモデルの開発研究が求められている．そこで，著者らは冠動脈結紮手法により，虚血部位を作製したモデルにおいて，長期的にその病態をフォローすることによりモデルの正当性の評価を試みた．図５に示した通り，心電図においてはSTの上昇が初期に認められ，さらに血液検査でもマーカーであるCPKやトロポニンT，BNPは病態を反映した値を示すなど，急性期におけるヒト同様の所見を示すことが明らかとなった．さらに，心エコーでは発症初期より長期的に左室の機能不全を認める

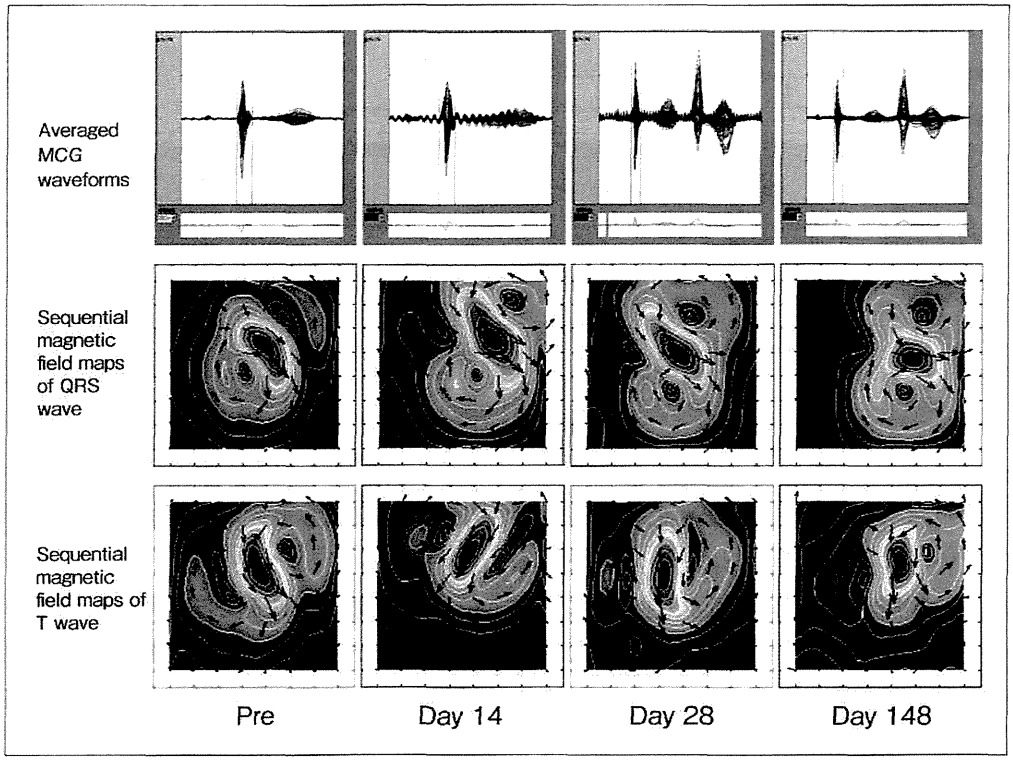


図６
心筋梗塞における心磁図アローマップ
脱分極時，再分極時の異常電流が梗塞直後から検出され，長期にわたって維持され続けた．

所見が観察された．また，病理所見でも虚血領域を中心とした心筋のリモデリング，線維化所見が認められ，ヒト病態を長期にわたり忠実に反映しているモデルであることが明らかとなった．

こうした心筋梗塞モデルに対し，前述の心磁計測を適応し，早期診断や予後判定のエビデンス確立も試みた．その結果，心磁図のアローマップでは梗塞所見を画像化することに成功し，さらに，それらを数値化して経時的な推移を追跡したところ，一度低下した数値は長期にわたって維持され，病態を反映し続けることが明らかとなった(図6)．すなわち，心筋梗塞に続発する慢性病態は心磁計によって非侵襲的に追跡評価が可能であることが示唆された．さらに，本モデルを使用した再生医療や遺伝子治療などの応用研究がこれまでに行われている[5]．

## Ⅶ．ま と め

現在，その他の霊長類循環器疾患モデルとして，バーストペーシングを応用した心不全モデル，心房細動モデル，人工心肺下の体外循環モデルなどの構築も進められている．いずれの疾患も患者数が多くQOLにも多大な影響を与え，社会的にも大きな問題となり，新規治療法開発が待たれていることから霊長類モデルの開発が急務となっている．さらに，われわれはこれまでに体外循環を利用した造血幹細胞移植モデル系も樹立してきた[6)～8)]．それに伴い，再生医療や遺伝子治療などの安全性・有効性評価が行われ，基礎と臨床をつなぐ応用研究の架け橋とされてきた[9)～11)]．

以上のように霊長類循環器疾患モデルを用いた研究の多くは現在も進行中であり，ヒトの新規診断・治療法の開発や病態メカニズムの解明がなされ，その成果が多くの研究に活かされることが期待されている．


## 謝　辞

本研究は多くの方々との共同研究の結果，得られた成果である．この場を借りて自治医科大学，日本大学，東北大学，岡山大学，筑波大学，三重大学，熊本大学，東京大学，国立国際医療研究センター，日立製作所および医薬基盤研究所の多くの共同研究者に心より感謝の意を表したい．


## 〔文　献〕


1) Koie H, Ageyama N, Ono F, Kanayama K, Sakai T, Sankai T : Echocardiographic diagnosis of muscular ventricular septal defect in a cynomolgus monkey (Macaca fascicularis). Contemp Top Lab Anim Sci, 2005 ; 44 : 26～28

2) Muneyuki K, Tsukada K, Seki Y, Kandori A, Ageyama N, Terao K : A comparison of magneto cardiograms of human and non-human primate. The Journal of Japan Biomagnetism and Bioelectromagnetics Society, 2007 ; 20 : 290～291

3) Seki Y, Muneyuki K, Kandori A, Tsukada K, Terao K, Ageyama N : Standardization of magnetocardiography in nonhuman primates. Phys Med Biol, 2008 ; 53 : 1609～1618

4) Ageyama N, Seki Y, Muneyuki K, Kandori A, Tsukada K, Terao K : Application of magnetocardiography for non-human primate arrythmia models. The Journal of Japan Biomagnetism and Bioelectromagnetics Society, 2007 ; 20 : 90～91

5) Yoshioka T, Ageyama N, Shibata H, Yasu T, Misawa Y, Takeuchi K, Matsui K, Yamamoto K, Terao K, Shimada K, Ikeda U, Ozawa K, Hanazono Y : Repair of infarcted myocardium mediated by transplanted bone marrow-derived CD34+stem cells in a nonhuman primate model. Stem Cells, 2005 ; 23 : 355～364

6) Ageyama N, Hanazono Y, Shibata H, Ono F, Ogawa H, Nagashima T, Ueda Y, Yoshikawa Y, Hasegawa M, Ozawa K, Terao K : Safe and efficient collection of cytokine-mobilized peripheral blood cells from cynomolgus monkeys (Macaca fascicularis) with human newborn-equivalent body weights. Exp Anim, 2005 ; 54 : 421～428

7) Ageyama N, Kimikawa M, Eguchi K, Ono F, Shibata H, Yoshikawa Y, Terao K : Modification of the leukapheresis procedure for use in rhesus monkeys (Macaca mulata). J Clin Apher, 2003 ; 18 : 26～31

8) Ageyama N, Hanazono Y, Shibata H, Ohto K, Ono F, Nagashima T, Ueda Y, Donahue RE, Hasegawa M, Ozawa K, Yoshikawa Y, Terao K : Safe and efficient methods of autologous hematopoietic stem cell transplantation for biomedical research in cynomolgus

monkeys. Comp Med, 2002 ; 52 : 445～451
9) Hanazono Y, Nagashima T, Takatoku M, Shibata H, Ageyama N, Asano T, Ueda Y, Dunbar CE, Kume A, Terao K, Hasegawa M, Ozawa K : In vivo selective expansion of gene-modified hematopoietic cells in a nonhuman primate model. Gene Ther, 2002 ; 9 : 1055～1064
10) Masuda S, Ageyama N, Shibata H, Obara Y, Ikeda T, Takeuchi K, Ueda Y, Ozawa K, Hanazono Y : Cotransplantation with MSCs improves engraftment of HSCs after autologous intra-bone marrow transplantation in nonhuman primates. Exp Hematol, 2009 ; 37 : 1250～1257
11) Chono H, Saito N, Tsuda H, Shibata H, Ageyama N, Terao K, Yasutomi Y, Mineno J, Kato I : In vivo safety and persistence of endoribonuclease gene-transduced CD4+ T cells in cynomolgus macaques for HIV-1 gene therapy model. PLoS One, 2011 ; 6 : e23585

---

T i t l e : Nonhuman Primate Models for Cardiovascular Diseases

Authors : Naohide Ageyama

Institute : Tsukuba Primate Research Center, National Institute of Biomedical Innovation

Cardiovascular Research (2013) **99**, 760–768
doi:10.1093/cvr/cvt163

# Blockade of sarcolemmal TRPV2 accumulation inhibits progression of dilated cardiomyopathy

**Yuko Iwata[1]*, Hitomi Ohtake[1], Osamu Suzuki[2], Junichiro Matsuda[2], Kazuo Komamura[3], and Shigeo Wakabayashi[1]**

[1]Department of Molecular Physiology, National Cerebral and Cardiovascular Center Research Institute, Fujishiro-dai 5-7-1, Suita, Osaka 565-8565, Japan; [2]Laboratory of Animal Models for Human Diseases, National Institute of Biomedical Innovation, Ibaraki, Osaka 567-0085, Japan; and [3]Department of Clinical Pharmacology and Pharmacogenomics, Graduate School of Pharmaceutical Science, Osaka University, Suita, Osaka 565-0871, Japan

*Received 23 January 2013; revised 1 June 2013; accepted 14 June 2013; online publish-ahead-of-print 19 June 2013*

**Time for primary review: 10 days**

**Aims** Dilated cardiomyopathy (DCM) is a severe disorder defined by ventricular dilation and contractile dysfunction. Abnormal $Ca^{2+}$ handling is hypothesized to play a critical pathological role in DCM progression. The transient receptor potential vanilloid 2 (TRPV2) has been previously suggested as a candidate pathway for enhanced $Ca^{2+}$ entry. Here, we examined the sarcolemmal accumulation of TRPV2 in various heart-failure model animals and DCM patients, and assessed whether presently available inhibitory tools against TRPV2 ameliorate DCM symptoms.

**Methods and results** Immunological and cell physiological analyses revealed that TRPV2 is highly concentrated and activated in the ventricular sarcolemma of DCM patients and three animal models—δ-sarcoglycan-deficient hamsters (J2N-k), transgenic mice over-expressing sialytransferase (4C30), and doxorubicin (DOX)-induced DCM mice. Over-expression of the amino-terminal (NT) domain of TRPV2 could block the plasma membrane accumulation and influx of $Ca^{2+}$ via TRPV2. Transgenic (Tg) or adenoviral expression of the NT domain in DCM animals caused effective removal of sarcolemmal TRPV2 along with reduction in the phosphorylation of calmodulin-dependent protein kinase II (CaMKII) and reactive oxygen species (ROS) production, which were activated in DCM; further, it prevented ventricular dilation and fibrosis, ameliorated contractile dysfunction in DCM, and improved survival of the affected animals. The TRPV2 inhibitor tranilast markedly suppressed DCM progression.

**Conclusion** Sarcolemmal TRPV2 accumulation appears to have considerable pathological impact on DCM progression, and blockade of this channel may be a promising therapeutic strategy for treating advanced heart failure.

**Keywords** Dilated cardiomyopathy • Heart failure • Therapeutic tool • $Ca^{2+}$-permeable channel • DOX-induced cardiomyopathy

## 1. Introduction

Dilated cardiomyopathy (DCM) is a severe disorder defined by ventricular dilation and cardiac dysfunction.[1–3] Although a considerable proportion of DCM cases develop because of inflammatory, metabolic, or toxic effects from medications, 30–48% of DCM cases are caused by genetic mutations.[4] Some affected genes encode sarcomeric or cytoskeletal proteins, including the components of the dystrophin–glycoprotein complex (DGC).[5,6] For example, δ-sarcoglycan-deficient hamsters (J2N-k) provide an animal model of human limb-girdle muscular dystrophy-associated DCM. However, little information is available regarding the pathways by which heterogeneous genetic defects and/or various causes lead to DCM symptoms.

The calcium ion ($Ca^{2+}$) plays a pivotal role in the pathogenesis of cardiac disease.[7,8] $Ca^{2+}$-handling abnormalities have been found in various forms of heart failure, including DCM.[9–11]

Further $Ca^{2+}$-permeable transient receptor potential (TRP) channels have recently been recognized as key molecules in pathological cardiac hypertrophy and heart failure.[12–14] We have previously reported that cardiac-specific over-expression of TRP vanilloid 2 (TRPV2) results in DCM with outstanding ventricular dilation,[15] suggesting that chronic elevation in cytosolic $Ca^{2+}$ concentrations ($[Ca^{2+}]_i$) is critical in DCM pathogenesis. However, it is unclear whether TRPV2 activity is a risk factor for DCM in humans as well as animals and whether TRPV2 inhibition can be beneficial against DCM progression, because of the limited number of methods for specific TRPV2 inhibition.

* Corresponding author. Tel: +81 6833 5012; fax: +81 6 6835 5314, Email: yukoiwat@ri.ncvc.go.jp

Therefore, we examined the role of TRPV2 in DCM. We also assessed the effect of TRPV2 blockades on cardiac dysfunction and DCM progression in several animal models.

# 2. Methods

Detailed methods are available in the Supplementary material online.

## 2.1 Molecular biology

All plasmid construction involving TRPV2 was carried out via a PCR-based strategy using the full-length mouse TRPV2 cDNA cloned into the pIRES expression vector (Invitrogen). Restriction enzyme-digested PCR products corresponding to the amino-terminal (NT) (amino acids (aa) 1–387) and carboxyl-terminal (CT) (aa 633–756) domains of TRPV2 were cloned into the p3Xflag-CMV-14 expression vector (Sigma-Aldrich). For adenoviral gene transfer, we inserted the haemagglutinin (HA)-tagged NT domain of TRPV2 (amino acids 1–387) cDNA into the pAd/CMV/V5-DEST viral vector (Invitrogen).

## 2.2 Animals and drug administration

DCM mice (4C30) were produced as described previously.[16] Heart-specific NT-transgenic (Tg) mice were generated from C57BL/6J mice according to the standard procedures.[15]

J2N-k hamsters, and age-matched normal controls (J2N-n) were purchased from Japan SLC. J2N-k hamsters were orally administered tranilast for 14 days at a dose of 30 or 300 mg/kg per day. In the DOX experiment, wild-type (WT) and NT-Tg mice were chronically treated with either phosphate-buffered saline (PBS; control) or doxorubicin (DOX) (Pfizer) by four intraperitoneal (i.p) injections (d 0, 2, 4, and 6) at a dose of 4 mg/kg (cumulative dose totalling 16 mg/kg). All animal experiments were performed in accordance with the Guidelines for Animal Experimentation of the National Cerebral and Cardiovascular Center (NCVC), and procedures were carried out in accordance with the Guide for the Care and Use of Laboratory Animals published by the US National Institutes of Health (NIH; NIH Publication, 8th Edition, 2011).

## 2.3 Histology, immunoblotting, and immunohistochemistry

Animals were anaesthetized with 5% isoflurane in an anaesthesia chamber until unresponsive to nose pinch, and the heart was harvested for

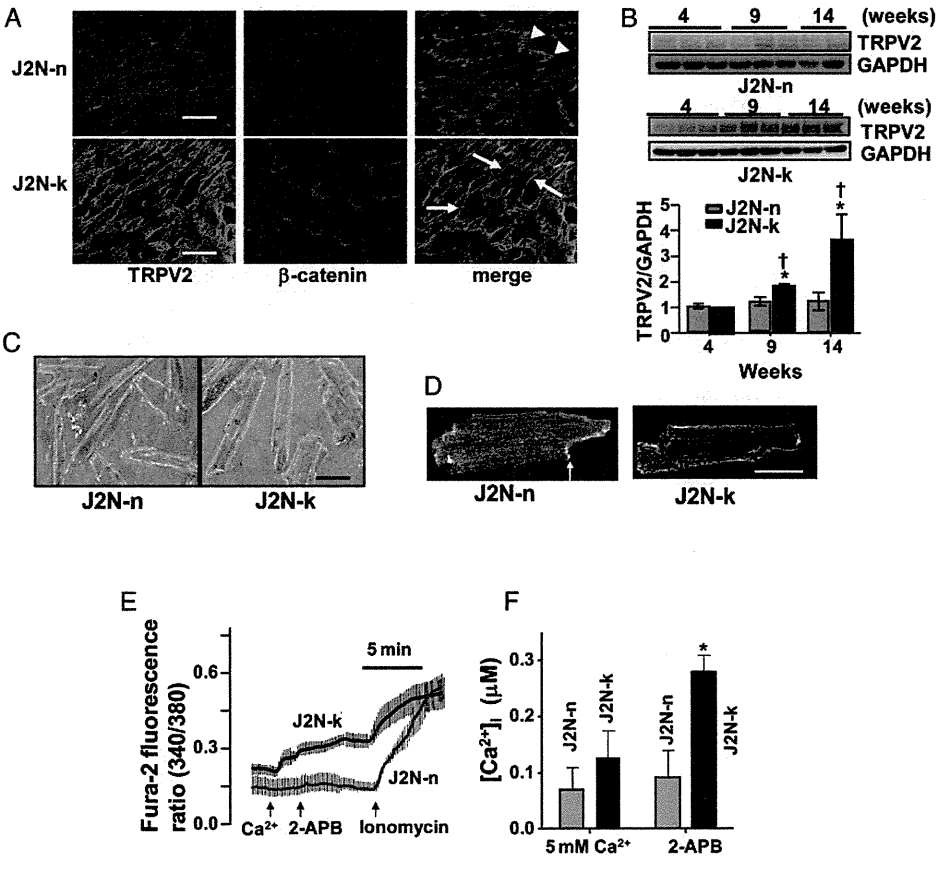


**Figure 1** TRPV2 accumulation and activation in the sarcolemma of cardiomyopathic hearts. (*A*) Immunohistochemical analysis of frozen ventricular sections from 8-week-old J2N-n and J2N-k hamsters with TRPV2 and β-catenin antibodies. β-catenin-positive intercalated discs or sarcolemmal regions are shown by arrowheads or arrows, respectively. Scale bar: 50 μm. (*B*) Immunoblots (40 μg/lane) of TRPV2-immunostained cardiac muscles. Age-dependent increases in the expression level of TRPV2 are observed. The data represent mean ± SD values ($n = 4–6$ hamsters/group); $^{*}P < 0.05$ vs. 4 weeks, $^{\dagger}P < 0.05$ vs. J2N-n. (*C*) Phase-contrast micrographs of freshly isolated ventricular cardiomyocytes. Scale bar: 30 μm. (*D*) Confocal micrographs of TRPV2-immunostained isolated cardiomyocytes. TRPV2 is extensively localized to the sarcolemma in J2N-k cells but to the intracellular compartment and intercalated disc (arrow) in J2N-n cells. Scale bar: 30 μm. (*E*) Intracellular $Ca^{2+}$ increase in response to extracellular $Ca^{2+}$ (5 mM) and 2-APB (500 μM) in cardiomyocytes loaded with fura-2. (*F*) Intracellular $Ca^{2+}$ concentration calculated from three independent experiments. The data represent mean ± SD values ($n = 7–10$ cardiomyocytes/group); $^{*}P < 0.05$.

biochemical assays. These experiments were conducted as described previously.[15,17,18]

### 2.4 Echocardiography

Cardiac function was evaluated by echocardiography using a Hewlett Packard Sonos 5500 ultrasound system with a 12-MHz transducer and M-mode imaging. Animals were sedated with tribromoethanol [i.p, 350 mg/kg of body weight (BW)] during the procedure.

### 2.5 Cardiomyocyte isolation and $[Ca^{2+}]_i$ measurement

Single-ventricular cardiomyocytes were freshly isolated from adult mouse and hamster hearts using standard enzymatic techniques.[19] The $[Ca^{2+}]_i$ was measured at room temperature via a ratiometric fluorescence method using fura-2 or indo-1 acetoxymethyl ester.[17,19]

### 2.6 Human tissues

Cardiac tissue samples were obtained from patients with DCM (Supplementary material online, *Table*). Written informed consent was obtained from all living patients, and the experiments on human tissues were approved by the Institutional Review Board of the NCVC. The investigation conforms to the principles of the Declaration of Helsinki.

### 2.7 Statistical analysis

We used an unpaired Student's *t*-test and one-way ANOVA followed by Dunnett's test for statistical analysis. $P < 0.05$ indicates statistical significance.

## 3. Results

### 3.1 TRPV2 is concentrated and activated in cardiomyopathic hearts

To study the role of TRPV2 in DCM, we first examined the expression and subcellular distribution of TRPV2 in the ventricles of δ-sarcoglycan-deficient (J2N-k) hamsters. In their normal control counterparts (J2N-n, 8-week-old hamsters), most of the TRPV2 expression was observed in the cell interior and in regions co-stained with the intercalated disc marker β-catenin (*Figure 1A*). In contrast, age-matched J2N-k ventricles showed increased TRPV2 expression in the peripheral sarcolemma as well as in parts of the intercalated discs (*Figure 1A*). With disease progression, total TRPV2 expression levels gradually increased only in J2N-k ventricles (from 9-week-old hamsters; *Figure 1B*). Although apparently similar rod shapes and sizes were noted in isolated cardiomyocytes from both types of hamsters (*Figure 1C*), stronger TRPV2 surface expression was observed in J2N-k cardiomyocytes than in controls (*Figure 1D*).

In J2N-k cardiomyocytes expressing TRPV2 in the sarcolemma, a rapid and large increase in $[Ca^{2+}]_i$ was elicited by exposure to the TRPV2 channel activator 2-aminoethoxydiphenyl borate (2-APB) as well as a high-$Ca^{2+}$ solution, whereas increases in $[Ca^{2+}]_i$ were marginal in control J2N-n cardiomyocytes (*Figure 1E* and *F*); this increase was inhibited by the TRPV channel antagonist ruthenium red (data not shown). Although TRPV1–3 are known to be activated by 2-APB, [20] cardiac tissues did not show detectable TRPV1 or TRPV3 expression (data not shown). Furthermore, although 2-APB is known to inhibit the intracellular $Ca^{2+}$-release channel inositol 1, 4, 5-trisphosphate receptor ($IP_3R$) and other TRP channel family proteins, [21] we saw an

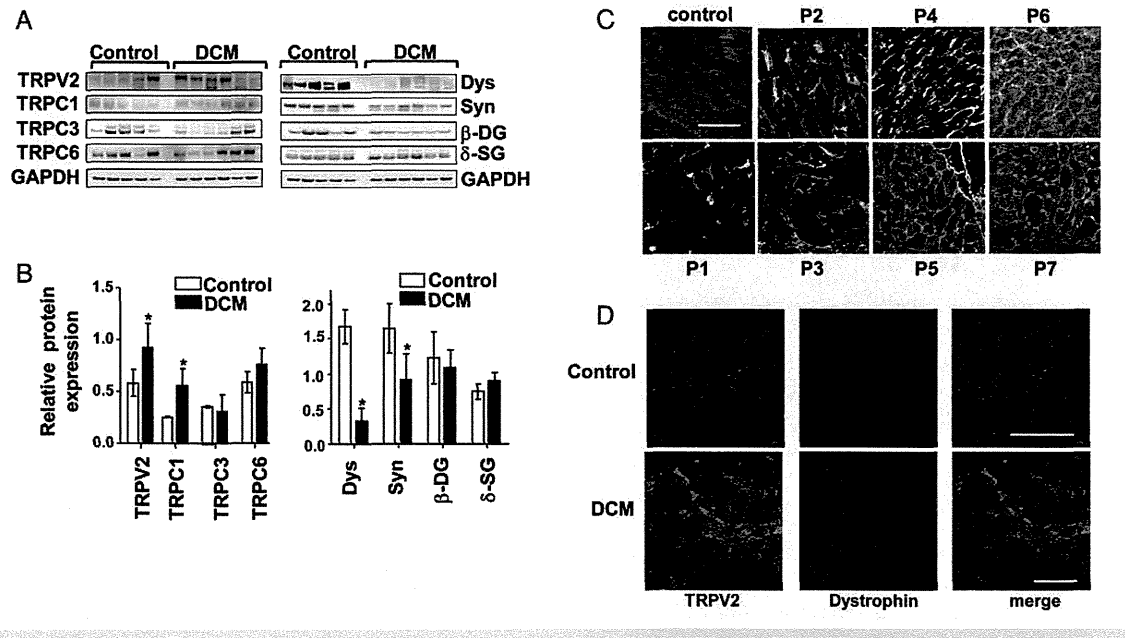


**Figure 2** Sarcolemmal TRPV2 accumulation in human DCM. (*A*) Representative immunoblot data of human heart homogenates. Controls and DCM patients; dys, dystrophin; syn, syntrophin; DG, dystroglycan; SG, sarcoglycan; TRPC, transient receptor potential canonical. (*B*) Protein expression levels relative to GAPDH expression in control (white bars) and patient (black bars) samples. The data represent mean ± SD values from four4 independent experiments ($n = 5–7$ samples/group); $^*P < 0.05$. (*C*) TRPV2 immunostaining of frozen human ventricular sections. P1–P7 (Supplementary material online, *Table S1*). Scale bar: 100 μm. (*D*) Ventricular sections from control and DCM patient were co-immunostained with TRPV2 and dystrophin. Note the surface localizsation of TRPV2 and reduced number of dystrophin-positive myocytes in DCM. Scale bar: 100 μm.

increase in $[Ca^{2+}]_i$, which is why TRPV2 was considered the principal candidate involved in the 2-APB-induced $[Ca^{2+}]_i$ increase in J2N-k cardiomyocytes. In addition, we observed that 2-APB often induced abnormal $Ca^{2+}$ elevation accompanied by loss of regular $Ca^{2+}$-transients under electrically stimulated conditions in J2N-k cardiomyocytes (but not in J2N-n control cardiomyocytes; unpublished observations). These data suggest that sarcolemmal TRPV2 accumulation contributes to the increased $[Ca^{2+}]_i$ levels in J2N-k cardiomyocytes.

In addition to the J2N-k hamster, other animal models with DCM display sarcolemmal accumulation of TRPV2. One such model is the 4C30 mouse, which over-expresses β-galactoside α-2,3-sialytransferase II (ST3Gal-II) and was recently developed as a model for human DCM; the other is DOX-induced DCM, a widely familiar model, although its precise mechanism of cardiotoxicity remains debatable. In hearts from these two animal models, total expression (see *Figures 4A* and *5E*) and sarcolemmal accumulation of TRPV2 (see *Figures 4B* and *5D* and Supplementary material online, *Figures S1* and *S2*) were found to be largely increased when compared with WT mice. In 4C30 mice, expression of TRP canonical (TRPC6), but not that of TRPC1 and TRPC3, was slightly increased (Supplementary material online, *Figure S3*); however, expression of α-dystroglycan and α-sarcoglycan were greatly reduced (Supplementary material online, *Figure S4*).

We next studied TRPV2 expression in ventricular samples from DCM patients (Supplementary material online, *Table S1*). TRPV2 and TRPC1 expression was significantly higher in DCM patients than in controls (*Figure 2A* and *B*), but expression of TRPC3 and TRPC6 was not significantly different. All DCM samples also exhibited reduced dystrophin and syntrophin expression levels (*Figure 2A* and *B*), suggesting that DCM is somehow linked to abnormal cytoskeletal organization. Similar to the findings in J2N-k ventricles, strong TRPV2 immunostaining was detected only in the peripheral sarcolemma of DCM cardiomyocytes (*Figure 2C*). Part of the TRPV2 expression was co-localized with the subsarcolemmal cytoskeletal protein dystrophin in human DCM ventricles, although dystrophin was detected only in a limited number of myocytes (*Figure 2D*).

## 3.2 Over-expression of the NT domain effectively blocks plasma membrane accumulation of TRPV2

We hypothesized that sarcolemmal TRPV2 accumulation is a common factor leading to $Ca^{2+}$-induced muscle degeneration in various heart diseases. Therefore, translocation of TRPV2 from the sarcolemma to the cell interior could be a promising therapeutic method. To study such 'back-translocation' of TRPV2, we used HEK293 cells, because they always recruit TRPV2 to the plasma membrane, independent of growth conditions, upon its heterologous expression (*Figure 3A*). We examined over-expression of several functional domains of TRPV2 together with full-length TRPV2 to identify the part of the TRPV2 molecule required for plasma membrane accumulation. We found that when the NT domain of TRPV2 was over-expressed, the majority of TRPV2 molecules moved from the sarcolemma to the cell interior (*Figure 3A*); such translocation was not observed with CT domain over-expression (*Figure 3A*). Consistent with this, over-expression of the NT but not the CT domain dramatically inhibited 2-APB-induced $[Ca^{2+}]_i$ increase (*Figure 3B* and *C*). Thus, the NT domain may be a useful tool for abrogating the sarcolemmal TRPV2 accumulation, thereby inhibiting the sustained increase in $[Ca^{2+}]_i$ in agonist-stimulated cells. To examine the effect of NT domain over-expression on DCM symptoms, we used 4C30 mice and DOX-induced DCM mice.

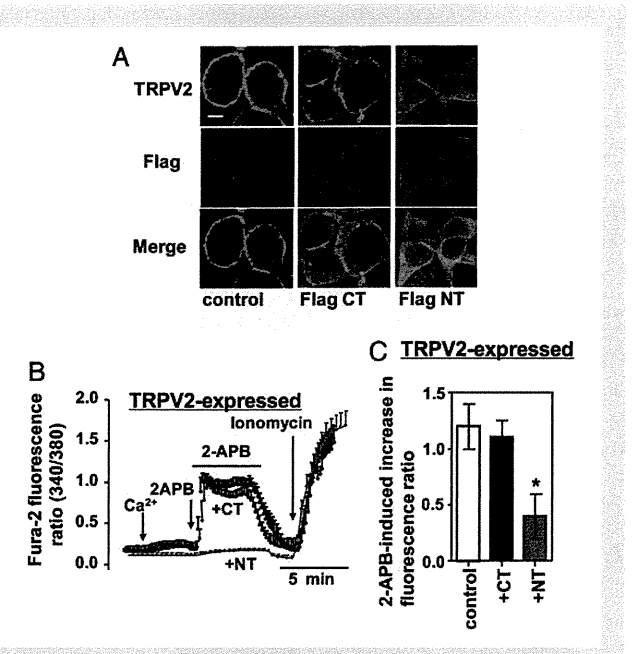


**Figure 3** Over-expression of the TRPV2 NT domain blocks the surface expression of TRPV2. (*A*) HEK293 cells expressing TRPV2 were transfected with Flag-tagged CT or NT domain and immunostained with anti-TRPV2 and anti-Flag antibodies. Note that the over-expression of the NT domain reduced TRPV2 surface expression. Scale bar: 10 μm. (*B*) Intracellular $Ca^{2+}$ increase in response to extracellular $Ca^{2+}$ (5 mM) and 2-APB (500 μM) in cells loaded with fura-2. (*C*) The peak fura-2 ratio induced by 2-APB was summarized from three independent experiments. The data represent mean ± SD values ($n$ = over 10 cells/group); $^*P < 0.05$.

## 3.3 Tg expression of the NT domain ameliorates cardiomyopathy in 4C30 mice

We generated Tg mice expressing the HA-tagged NT domain (*Figure 4A*) under the control of the α-myosin heavy chain (α-MHC) promoter. NT-Tg mice were apparently healthy as evidenced by normal heart morphology (*Figure 4C*), cardiac function (*Figure 4G* and *H*) and life span (*Figure 4I*). The NT domain was introduced into the hearts of 4C30 mice by crossing them with NT-Tg mice. Interestingly, elevated expression level of endogenous TRPV2 in 4C30 mice was decreased to control levels in 4C30/NT-Tg mice (*Figure 4A*). The exogenous NT domain was mostly localized to intercalated discs in both NT-Tg and 4C30/NT-Tg mice (*Figure 4B*). As expected, the sarcolemmal localization of TRPV2 in 4C30 mice was dramatically reduced following NT domain over-expression (4C30/NT-Tg) (*Figure 4B*), potentially leading to a reduction in sustained $[Ca^{2+}]_i$ increase. Consistent with this idea, CaMKII phosphorylation was markedly reduced in the 4C30/NT-Tg mice (*Figure 4A*). In addition, the expression level of modulatory calcineurin inhibitory protein-1 (MCIP) was increased in 4C30 mice but reduced in 4C30/NT-Tg mice (*Figure 4A*), further suggesting that blockade of TRPV2 results in a reduction in sustained $[Ca^{2+}]_i$ increase.

In 4C30 mice aged more than 120 days, we observed thinner ventricular walls and greater ventricular dilation accompanied by fibrosis (*Figure 4C*), with increased serum cardiac troponin I (cTnI; a heart

injury marker) levels (*Figure 4D*). Furthermore, reactive oxygen species (ROS) production measured by dihydroethidium (DHE) staining (*Figure 4E*) and the extent of lipid peroxidation estimated by measurement of 4-hydroxynonenal (4-HNE) adducts (*Figure 4F*) were significantly higher in the 4C30 mice, suggesting high oxidative stress in these DCM hearts. The 4C30/NT-Tg mice showed marked suppression of these symptoms (*Figure 4C–F*). Echocardiographically, the 4C30 mice showed increased left-ventricular diastolic and systolic dimensions (LVDd and LVDs, respectively), with decreased fractional shortening (FS) and ejection fractions (EF) (*Figure 4G* and *H*). However, the 4C30/NT-Tg mice had significantly improved cardiac functions. Moreover, the 4C30 mice progressively died at 200–300 days after birth, but 4C30/NT-Tg mice had a much longer life span, particularly the female mice (*Figure 4I*). We suspect that the amelioration in DCM symptoms may have resulted from the removal of endogenous TRPV2 from the sarcolemma.

## 3.4 Beneficial effects of NT domain over-expression in DOX-induced DCM

The effects of NT domain over-expression were next examined in DOX-induced DCM. In WT mice, DOX treatment resulted in ventricular dilation, reduced FS, and higher mortality (*Figure 5A–C*). In contrast, DOX-treated NT-Tg mice demonstrated better cardiac morphology and function and better survival (*Figure 5A–C*). Indeed, upon DOX treatment, the NT-Tg mice showed lower TRPV2 expression and sarcolemmal accumulation of TRPV2 (*Figure 5D* and *E*), demonstrating reduced CaMKII phosphorylation (*Figure 5E*) and oxidative stress (*Figure 5F* and *G*). These results suggest that TRPV2 also plays an important pathological role in non-genetic heart failure, such as DOX-induced DCM.

## 3.5 Adenoviral expression of the NT domain ameliorates cardiac dysfunction in J2N-k hamsters

We next addressed whether the effects of the NT domain could be seen in J2N-k cardiomyopathy following over-expression via adenoviral transfer. We injected an adenovirus carrying either β-galactosidase (β-gal; as a control) or the NT domain into the hearts of 9-week-old J2N-k hamsters, at which age sarcolemmal TRPV2 translocation and cardiac dysfunction had already been observed. At 14 days post-injection, we detected NT domain expression in the ventricles by immunoblotting with the HA antibody (*Figure 6A*). Detection of green fluorescent protein (GFP) in cardiac homogenates (*Figure 6A*) and sections (*Figure 6B*) confirmed that the adenoviral vector had reached the

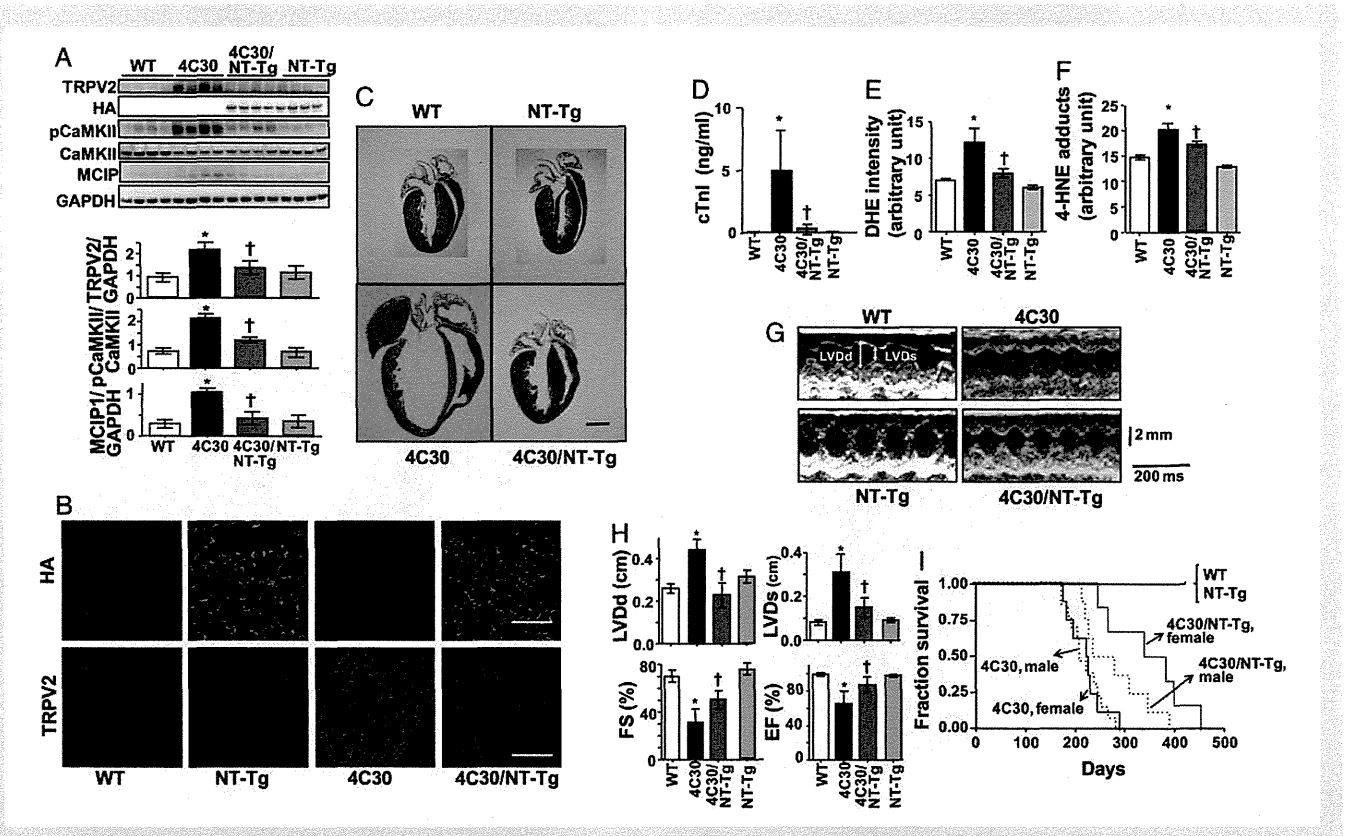


**Figure 4** Over-expression of the NT domain blocks TRPV2 surface expression and ameliorates morphological and biochemical symptoms of cardiomyopathy in 4C30 mice. (*A*) Representative immunoblot of heart homogenates with the indicated antibodies (upper panel). Data represent values from four independent experiments ($n = 3–4$/group) $^{*}P < 0.05$ vs. WT mice, $^{\dagger}P < 0.05$ vs. 4C30 mice. (*B*) Representative immunohistochemical data from longitudinal cardiac sections from each group of mice. Scale bar: 100 μm. (*C*) Cardiac sections from 150-day-old mice stained with Masson's trichrome. Scale bar: 5 mm. (*D*) Level of cTnI in serum ($n = 10$ mice/group). (*E*) Superoxides produced in the hearts were analysed by staining the ventricular tissues with DHE. (*F*) Immunostaining data of the hearts with 4-HNE antibody were analysed ($n = 3$ mice/group) $^{*}P < 0.05$ vs. WT mice, $^{\dagger}P < 0.05$ vs. 4C30 mice. (*G*) Representative echocardiograms of each group of mice. (*H*) Echocardiographic analysis of cardiac function. (*I*) Kaplan–Meier survival analysis of each group of mice ($n = 25–30$ mice/group).

cardiac muscles and that the surface membrane expression of TRPV2 was decreased by NT domain over-expression. Echocardiography revealed that NT domain over-expression resulted in good amelioration of cardiac dysfunction, with improved FS and EF and reduced fibrosis (*Figure 6C–E*). These results demonstrated that NT domain-induced prevention of the sarcolemmal localization of TRPV2 can greatly ameliorate gene-defective DCM.

### 3.6 Tranilast prevents cardiomyopathy in J2N-k hamsters

We previously found that tranilast, which is known to be a non-selective cation channel blocker, effectively inhibits TRPV2.[22] Tranilast inhibited 2-APB-induced $[Ca^{2+}]_i$ increases with half-maximal inhibition at about 30 μM, in HEK293 cells expressing TRPV2 (Supplementary material online, *Figure S5*), but it has almost no effect on HEK293 cells expressing TRPV1, TRPV3, or TRPC1 (Supplementary material online, *Figure S5*). A recent study reported that tranilast inhibits TRPV2 ion channel activity.[23] Thus, tranilast is one of the better inhibitors presently available against TRPV2. We observed that tranilast reduced the amount of surface TRPV2 and abnormal $Ca^{2+}$ mobilization by 2-APB in DCM cardiomyocytes (J2N-k, 4C30; unpublished observation). Oral administration of tranilast to J2N-k hamsters resulted in the effective removal of TRPV2 from the sarcolemma of J2N-k hearts (*Figure 6F*), similar to the effect of TRPV2 NT domain over-expression. Tranilast markedly reduced ventricular dilation and muscle fibrosis in J2N-k hearts (*Figure 6G*). Furthermore, it improved cardiac contraction, as evidenced by a decrease in echocardiographic parameters (LVDd and LVDs) to control levels (*Figure 6H*) and improved FS (*Figure 6H*).

## 4. Discussion

The present results suggest, for the first time, the pathological significance of TRPV2 in DCM development. First, TRPV2 was observed to be extensively localized to the ventricular sarcolemma in DCM patients as well as in animal models of heart failure (J2N-k, 4C30, and DOX-induced cardiomyopathic mice), whereas it localized to the intracellular compartments and intercalated discs in normal ventricles. Second, Tg or adenoviral NT domain over-expression significantly reduced the sarcolemmal accumulation of TRPV2 and simultaneously ameliorated cardiac dysfunction, preventing DCM progression and improving survival in the animal models. Third, the TRPV2 inhibitor tranilast effectively prevented DCM progression in J2N-k hamsters. Based on these findings, we

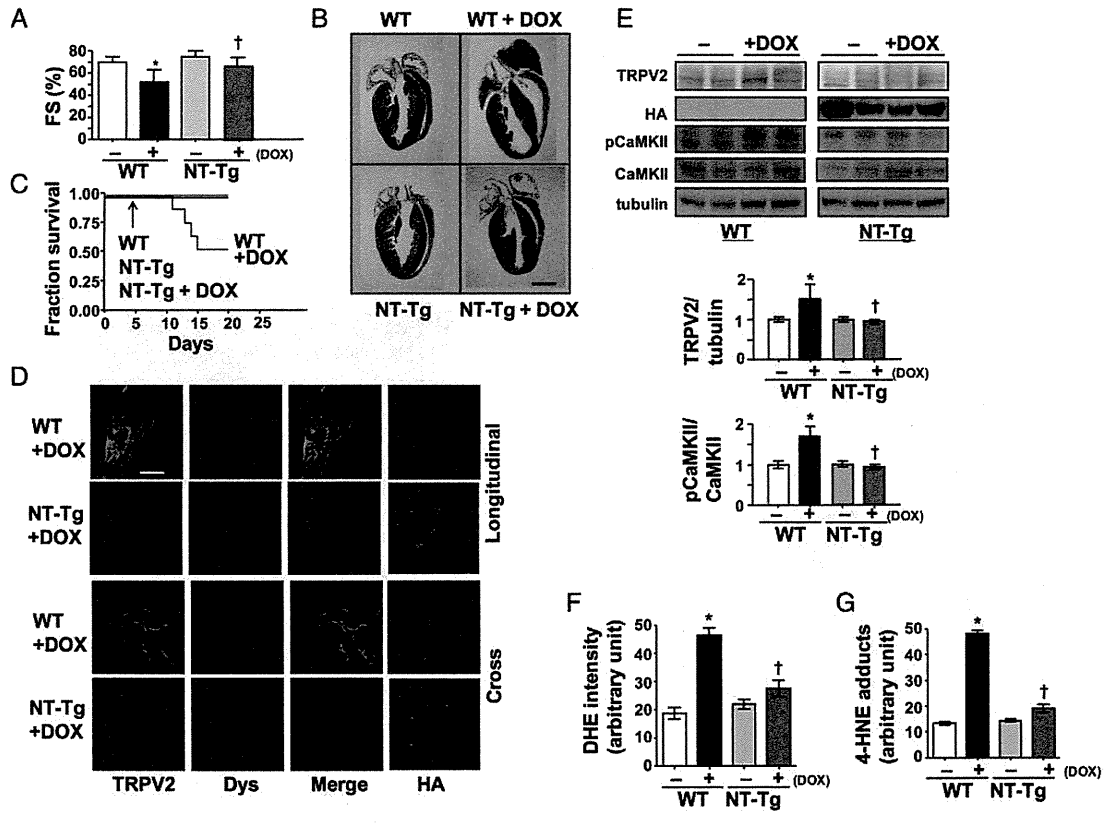


**Figure 5** Over-expression of the NT domain ameliorates DOX-induced cardiomyopathy. (*A*) Echocardiographic analysis of cardiac function ($n = 6$ mice/group); $^*P < 0.05$ vs. without DOX, $^\dagger P < 0.05$ vs. WT with DOX. (*B*) Cardiac sections from 11-week-old DOX-treated or untreated WT or NT-Tg mice were stained with Masson's trichrome. Scale bar: 5 mm. (*C*) Kaplan–Meier survival analysis of each group of mice ($n = 15$ mice/group). (*D*) Immunohistochemical analysis of longitudinal (upper panel) and cross-sections (lower panel) of hearts from each group of mice. Scale bar: 100 μm. TRPV2, dystrophin (Dys) and HA antibodies were used. (*E*) Representative immunoblot data of heart homogenates from DOX-treated or untreated WT mice or NT-Tg with the indicated antibodies (left). TRPV2 expression levels are shown relative to tubulin expression and the extent of CaMKII phosphorylation is shown relative to total CaMKII levels (right). The data represent values from three independent experiments. (*F* and *G*) Levels of oxidative stress markers ($n = 4$ mice/group), $^*P < 0.05$ vs. without DOX, $^\dagger P < 0.05$ vs. WT with DOX.

hypothesize that the amelioration of DCM resulted from the inhibition of the $Ca^{2+}$ influx through TRPV2; therefore, TRPV2 may be a potential upstream target against abnormal $Ca^{2+}$ handling.

The DCM phenotype results from a broad variety of primary and secondary aetiologies. Despite the various underlying causes, there are many similarities in the final structural, functional, biochemical, and molecular phenotypes related to the long-lasting mechanical stress and neurohormonal activation observed in DCM.[24] CaMKII is an ideal nodal molecule for transducing $Ca^{2+}$ signals into downstream events such as apoptosis and necrosis, leading to clinical phenotypes of congestive heart failure and sudden death.[25] In addition to CaMKII activation, ROS production is frequently observed in DCM hearts, with detrimental effects on cardiomyocytes.[26] We found that increased CaMKII phosphorylation and ROS production observed in DCM hearts were attenuated by over-expression of the NT domain of TRPV2 (*Figures 4* and *5*), suggesting that TRPV2 may be an upstream regulator of $Ca^{2+}$ influx and ROS production as well as an important mediator of various stress signals, including those arising from genetic defects, mechanical stress, and cardiotoxic drugs, leading to $Ca^{2+}$-induced cell death. In addition, calcineurin is known to be an important $Ca^{2+}$-dependent signalling molecule leading to cardiac hypertrophy.[27] Certainly, cardiomyocyte-specific over-expression of calcineurin causes hypertrophy [28] and cardiomyopathy, but conflicting results are reported on the effects of calcineurin inhibition.[29] In our DCM models, calcineurin was slightly activated, as determined by the increase in the expression level of MCIP protein (*Figure 4*) as well as CaMKII activation and inhibition of TRPV2 suppressed both $Ca^{2+}$-signalling pathways (*Figure 4*). These findings suggest TRPV2 as a putative therapeutic target for the treatment of heart failure.

Here, we used 4C30 mice as a model for human idiopathic DCM. Unlike J2N-k hamsters, which gradually develop DCM, 4C30 mice are apparently asymptomatic up to 100 days but thereafter rapidly exhibit DCM symptoms and die within 200 days. Similar to that in 4C30 mice,[16] sialytransferase expression levels are altered in human DCM.[30] 4C30 mice also show DGC abnormalities (Supplementary material online, *Figure S4*), similar to those in DCM patients (*Figure 2A* and *B*). These characteristics indicate a pointed resemblance between 4C30 mice and human idiopathic DCM. Dystrophin degradation by the $Ca^{2+}$-dependent protease calpain was proposed as a pathway in



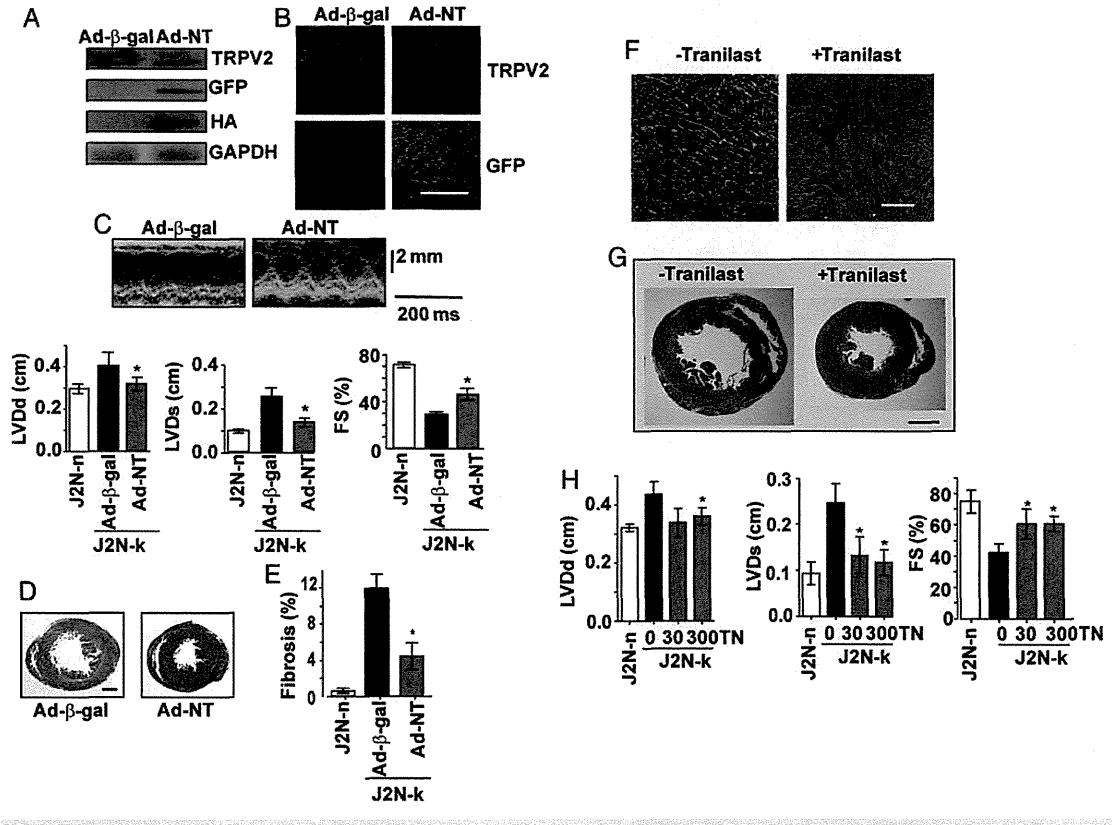


**Figure 6** Two inhibitory tools against TRPV2 show comparative amelioration of cardiomyopathy in J2N-k. (*A*) Representative immunoblot and (*B*) immunohistochemical data of heart homogenates or sections from 11-week-old J2N-k infected with adenovirus carrying β-galactosidase (Ad-β-gal, control) or the NT domain (Ad-NT). Adenoviral infection was confirmed by staining with GFP. Scale bar: 100 μm. Similar results were obtained from three independent experiments. (*C*) Echocardiographic analysis of adenovirus-infected J2N-k. Representative echocardiograms (upper panels) and statistical evaluation (lower panels; $n = 6$ hearts/group); $^*P < 0.05$ vs. control. (*D*) Masson's trichrome staining of cardiac sections from adenovirus-infected J2N-k. (*E*) Fibrotic areas were analysed ($n = 6$ hearts/group). (*F*) J2N-k hamsters were administered none (−) or (+) tranilast (300 mg/kg per day) for 2 weeks, and the obtained tissues were immunostained with TRPV2 antibody. Tranilast prevented the sarcolemmal accumulation of TRPV2. Scale bar: 100 μm. (*G*) Heart sections from J2N-k hamsters were stained with Masson's trichrome. Tranilast ameliorated ventricular dilation and reduced fibrosis in these hamsters. Scale bar: 5 mm. (*H*) Effect of tranilast (TN) (0, 30, 300 mg/kg) on echocardiographic parameters in J2N-k ($n = 5–8$ hamsters/group); $^*P < 0.05$ vs. no treatment in J2N-k.

advanced heart failure with DCM symptoms.[31] Therefore, TRPV2 remodelling appears to be linked to sarcolemmal instability caused by DGC defects in various models of advanced heart failure. Thus, the 4C30 mouse appears to be a good animal model to study the connection between $Ca^{2+}$ abnormality and DCM symptoms.

Plasma membrane TRPV2 translocation is known to be stimulated by receptor agonists[15,32] or mechanical stress.[15] Stimulation by growth factors or sympathetic transmitters could act as a signal inducing sarcolemmal TRPV2 translocation in DCM, because these stimulants are known to be released into the blood vessels of diseased hearts in response to mechanical load.[33] Considering that the TRPV2 inhibitory tools abrogated the surface expression of TRPV2 (*Figure 6*), $Ca^{2+}$ influx via TRPV2 may also be important for sarcolemmal TRPV2 accumulation. Although further confirmatory studies are required, we suspect that NT domain over-expression inhibited membrane retention of TRPV2 by disrupting the interaction between TRPV2 and its putative binding partner, which regulates subcellular localization. Recently, a peptide mimetic of the CT domain of connexin 43 was used to disrupt the interaction between connexin 43 and the PDZ2 domain of zonula occludens-1 and reduce gap junction remodelling in injured hearts.[34]

Tranilast prevented ventricular dilation and fibrosis and ameliorated decreased FS by ~50% in J2N-k hamsters (*Figure 6*). These beneficial effects were comparable to those obtained from the adenoviral transfer of the NT domain (*Figure 6*). These treatments were performed in 9-week-old J2N-k hamsters that had already started displaying DCM symptoms. Therefore, our approach may be useful as a therapeutic intervention against the initial symptoms of DCM. Similar results using different strategies (chemical vs. protein) strongly suggest that TRPV2 activity contributes to DCM progression. Importantly, tranilast is immediately available for patients as an anti-inflammatory compound, since it reportedly has anti-inflammatory and immunomodulatory effects;[35] therefore, it may have clinical potential in DCM therapy. Recently, consistent with our data, tranilast has been reported to reduce both functional and structural abnormalities in diabetic cardiomyopathic rats[36] and prevent the progression from compensated hypertrophy to heart failure in pressure-overloaded mice.[37] The latter study suggested that tranilast reduced the heart-failure progression by acting as a mast-cell stabilizer. Since TRPV2 was reported to be involved in mast-cell degranulation,[38] TRPV2 may be also responsible for tranilast-induced amelioration of heart failure.

In conclusion, specific abrogation of TRPV2 activity by either NT domain over-expression or chemical inhibitor treatment led to considerable amelioration of cardiac pathology in the animal models. Our findings strongly suggest that the sarcolemmal TRPV2 accumulation plays a crucial role in $Ca^{2+}$-induced muscle degeneration in DCM and that TRPV2 is a good therapeutic target for advanced heart failure.

## Supplementary material

Supplementary material is available at *Cardiovascular Research* online.

## Acknowledgements

We thank Dr Hatsue Ueda (NCVC) for kindly providing us with information for human samples and Dr Yuji Arai (NCVC) for technical support in Tg production.

**Conflict of interest:** none declared.

## Funding

This work was supported by a Grant-in-Aid for Priority Areas (grant number 18077015) to S.W.; Grants-in-Aid (grant numbers 19390080, 17659241 (to S.W.), 18590796, 20590874 (to Y.I.)); and a Grants-in-Aid (grant number 22659046) for Exploratory Research to S.W. from the Japanese Ministry of Education, Culture, Sports, Science and Technology; a grant for the Promotion of Fundamental Studies in Health Sciences of the National Institute of Biomedical Innovation; research grants for Cardiovascular Diseases (grant number 17A-1) to S.W. and Nervous and Mental Disorders (grant numbers 16B-2 and 19A-7) to Y.I. from the Japanese Ministry of Health, Labour and Welfare.

## References

1. Hughes SE, McKenna WJ. New insights into the pathology of inherited cardiomyopathy. *Heart* 2005;**91**:257–264.
2. Fatkin D, Graham RM. Molecular mechanisms of inherited cardiomyopathies. *Physiol Rev* 2002;**82**:945–980.
3. Seidman JG, Seidman C. The genetic basis for cardiomyopathy: from mutation identification to mechanistic paradigms. *Cell* 2001;**104**:557–567.
4. Jefferies JL, Towbin JA. Dilated cardiomyopathy. *Lancet* 2010;**375**:752–762.
5. Campbell KP, Kahl SD. Association of dystrophin and an integral membrane glycoprotein. *Nature* 1989;**338**:259–262.
6. Nigro V, Okazaki Y, Belsito A, Piluso G, Matsuda Y, Politano L *et al.* Identification of the Syrian hamster cardiomyopathy gene. *Hum Mol Genet* 1997;**6**:601–607.
7. Jeong EM, Liu M, Sturdy M, Gao G, Varghese ST, Sovari AA *et al.* Metabolic stress, reactive oxygen species, and arrhythmia. *J Mol Cell Cardiol* 2012;**52**:454–463.
8. Toko H, Takahashi H, Kayama Y, Oka T, Minamino T, Okada S *et al.* $Ca^{2+}$/calmodulin-dependent kinase IIdelta causes heart failure by accumulation of p53 in dilated cardiomyopathy. *Circulation* 2010;**122**:891–899.
9. Beuckelmann DJ, Nabauer M, Erdmann E. Intracellular calcium handling in isolated ventricular myocytes from patients with terminal heart failure. *Circulation* 1992;**85**:1046–1055.
10. Lindner M, Brandt MC, Sauer H, Hescheler J, Bohle T, Beuckelmann DJ. Calcium sparks in human ventricular cardiomyocytes from patients with terminal heart failure. *Cell Calcium* 2002;**31**:175–182.
11. Louch WE, Bito V, Heinzel FR, Macianskiene R, Vanhaecke J, Flameng W *et al.* Reduced synchrony of $Ca^{2+}$ release with loss of T-tubules-a comparison to $Ca^{2+}$ release in human failing cardiomyocytes. *Cardiovascular Research* 2004;**62**:63–73.
12. Eder P, Molkentin JD. TRPC channels as effectors of cardiac hypertrophy. *Circ Res* 2011;**108**:265–272.
13. Nilius B, Owsianik G, Voets T, Peters JA. Transient receptor potential cation channels in disease. *Physiol Rev* 2007;**87**:165–217.
14. Watanabe H, Murakami M, Ohba T, Takahashi Y, Ito H. TRP channel and cardiovascular disease. *Pharmacol Therap* 2008;**118**:337–351.
15. Iwata Y, Katanosaka Y, Arai Y, Komamura K, Miyatake K, Shigekawa M. A novel mechanism of myocyte degeneration involving the $Ca^{2+}$-permeable growth factor-regulated channel. *J Cell Biol* 2003;**161**:957–967.
16. Suzuki O, Kanai T, Nishikawa T, Yamamoto Y, Noguchi A, Takimoto K *et al.* Adult onset cardiac dilatation in a transgenic mouse line with Galβ1,3GalNAc α2,3-sialyltransferase II (ST3Gal-II) transgenes: a new model for dilated cardiomyopathy. *Proc Japan Acad, SerB* 2011;**87**:550–562.
17. Iwata Y, Katanosaka Y, Arai Y, Shigekawa M, Wakabayashi S. Dominant-negative inhibition of Ca2+ influx via TRPV2 ameliorates muscular dystrophy in animal models. *Hum Mol Genet* 2009;**18**:824–834.
18. Iwata Y, Pan Y, Hanada H, Yoshida T, Shigekawa M. Dystrophin-glycoprotein complex purified from hamster cardiac muscle. Comparison of the complexes from cardiac and skeletal muscles of hamster and rabbit. *J Mol Cell Cardiol* 1996;**28**:2501–2509.
19. Nakamura TY, Iwata Y, Arai Y, Komamura K, Wakabayashi S. Activation of $Na^+/H^+$ exchanger 1 is sufficient to generate $Ca^{2+}$ signals that induce cardiac hypertrophy and heart failure. *Circ Res* 2008;**103**:891–899.
20. Hu HZ, Gu Q, Wang C, Colton CK, Tang J, Kinoshita-Kawada M *et al.* 2-aminoethoxydiphenyl borate is a common activator of TRPV1, TRPV2, and TRPV3. *J Biol Chem* 2004;**279**:35741–35748.
21. Lievremont JP, Bird GS, Putney JW Jr. Mechanism of inhibition of TRPC cation channels by 2-aminoethoxydiphenylborane. *Mol Pharmacol* 2005;**68**:758–762.
22. Iwata Y, Katanosaka Y, Shijun Z, Kobayashi Y, Hanada H, Shigekawa M *et al.* Protective effects of $Ca^{2+}$ handling drugs against abnormal $Ca^{2+}$ homeostasis and cell damage in myopathic skeletal muscle cells. *Biochem Pharmacol* 2005;**70**:740–751.
23. Mihara H, Boudaka A, Shibasaki K, Yamanaka A, Sugiyama T, Tominaga M. Involvement of TRPV2 activation in intestinal movement through nitric oxide production in mice. *J Neurosci* 2010;**30**:16536–16544.
24. Houser SR, Margulies KB, Murphy AM, Spinale FG, Francis GS, Prabhu SD *et al.* Animal models of heart failure: a scientific statement from the American Heart Association. *Circ Res* 2012;**111**:131–150.

25. Anderson ME. CaMKII and a failing strategy for growth in heart. *J Clin Invest* 2009;**119**: 1082–1085.
26. Giordano FJ. Oxygen, oxidative stress, hypoxia, and heart failure. *J Clin Invest* 2005;**115**: 500–508.
27. Wilkins BJ, Dai YS, Bueno OF, Parsons SA, Xu J, Plank DM *et al.* Calcineurin/NFAT coupling participates in pathological, but not physiological, cardiac hypertrophy. *Circ Res* 2004; **94**:110–118.
28. Molkentin JD, Lu JR, Antos CL, Markham B, Richardson J, Robbins J *et al.* A calcineurin-dependent transcriptional pathway for cardiac hypertrophy. *Cell* 1998;**93**:215–228.
29. Wilkins BJ, Molkentin JD. Calcium-calcineurin signaling in the regulation of cardiac hypertrophy. *Biochem Biophys Res Commun* 2004;**322**:1178–1191.
30. Hwang JJ, Allen PD, Tseng GC, Lam CW, Fananapazir L, Dzau VJ *et al.* Microarray gene expression profiles in dilated and hypertrophic cardiomyopathic end-stage heart failure. *Physiol Genom* 2002;**10**:31–44.
31. Toyo-Oka T, Kawada T, Nakata J, Xie H, Urabe M, Masui F *et al.* Translocation and cleavage of myocardial dystrophin as a common pathway to advanced heart failure: a scheme for the progression of cardiac dysfunction. *Proc Natl Acad Sci USA* 2004;**101**:7381–7385.
32. Kanzaki M, Zhang YQ, Mashima H, Li L, Shibata H, Kojima I. Translocation of a calcium-permeable cation channel induced by insulin-like growth factor-I. *Nat Cell Biol* 1999;**1**: 165–170.
33. Ruwhof C, van der Laarse A. Mechanical stress-induced cardiac hypertrophy: mechanisms and signal transduction pathways. *Cardiovasc Res* 2000;**47**:23–37.
34. O'Quinn MP, Palatinus JA, Harris BS, Hewett KW, Gourdie RG. A peptide mimetic of the connexin43 carboxyl terminus reduces gap junction remodeling and induced arrhythmia following ventricular injury. *Circ Res* 2011;**108**:704–715.
35. Pae HO, Jeong SO, Koo BS, Ha HY, Lee KM, Chung HT. Tranilast, an orally active anti-allergic drug, up-regulates the anti-inflammatory heme oxygenase-1 expression but down-regulates the pro-inflammatory cyclooxygenase-2 and inducible nitric oxide synthase expression in RAW264.7 macrophages. *Biochem Biophys Res Commun* 2008;**371**: 361–365.
36. Kelly DJ, Zhang Y, Connelly K, Cox AJ, Martin J, Krum H *et al.* Tranilast attenuates diastolic dysfunction and structural injury in experimental diabetic cardiomyopathy. *Am J Physiol Heart Circ Physiol* 2007;**293**:H2860–H2869.
37. Hara M, Ono K, Hwang MW, Iwasaki A, Okada M, Nakatani K *et al.* Evidence for a role of mast cells in the evolution to congestive heart failure. *J Exp Med* 2002;**195**: 375–381.
38. Zhang D, Spielmann A, Wang L, Ding G, Huang F, Gu Q *et al.* Mast-cell degranulation induced by physical stimuli involves the activation of transient-receptor-potential channel TRPV2. *Physiol Res* 2012;**61**:113–124.

*Exp. Anim. 62(3), 267–273, 2013*

—Original—

# Zygosity Determination in Hairless Mice by PCR Based on *Hr*$^{hr}$ Gene Analysis

Osamu SUZUKI, Minako KOURA, Yoko NOGUCHI, Kozue UCHIO-YAMADA, and Junichiro MATSUDA

*Laboratory of Animal Models for Human Diseases, National Institute of Biomedical Innovation, 7–6–8 Saito-Asagi, Ibaraki, Osaka 567-0085, Japan*

**Abstract:** We analyzed the *Hr* gene of a hairless mouse strain of unknown origin (HR strain, http://animal.nibio.go.jp/e_hr.html) to determine whether the strain shares a mutation with other hairless strains, such as HRS/J and Skh:HR-1, both of which have an *Hr*$^{hr}$ allele. Using PCR with multiple pairs of primers designed to amplify multiple overlapping regions covering the entire *Hr* gene, we found an insertion mutation in intron 6 of mutant *Hr* genes in HR mice. The DNA sequence flanking the mutation indicated that the mutation in HR mice was the same as that of *Hr*$^{hr}$ in the HRS/J strain. Based on the sequence, we developed a genotyping method using PCR to determine zygosities. Three primers were designed: S776 (GGTCTCGCTGGTCCTTGA), S607 (TCTGGAACCAGAGTGACAGACAGCTA), and R850 (TGGGCCACCATGGCCAGATTTAACACA). The S776 and R850 primers detected the *Hr*$^{hr}$ allele (275-bp amplicon), and S607 and R850 identified the wild-type *Hr* allele (244-bp amplicon). Applying PCR using these three primers, we confirmed that it is possible to differentiate among homozygous *Hr*$^{hr}$ (longer amplicons only), homozygous wild-type *Hr*(shorter amplicons only), and heterozygous (both amplicons) in HR and Hos:HR-1 mice. Our genomic analysis indicated that the HR, HRS/J, and Hos:HR-1 strains, and possibly Skh:HR-1 (an ancestor of Hos:HR-1) strain share the same *Hr*$^{hr}$ gene mutation. Our genotyping method will facilitate further research using hairless mice, and especially immature mice, because pups can be genotyped before their phenotype (hair coat loss) appears at about 2 weeks of age.

**Key words:** hairless, genome, genotyping, mice, zygosity

## Introduction

Many hairless mouse strains such as HRS/J and Skh:HR-1 are often used in studies of skin, cancer, and immunology by Benavides *et al.* [3] and Sundberg [12]. At our institute, we have been maintaining a hairless mouse strain of unknown origin called HR (http://animal.nibio.go.jp/e_hr.html). It was introduced from a University in California (there is no precise university name in our records) to Yokohama City University in 1964. The strain was then introduced in 1965 to the Institute of Medical Science of the University of Tokyo, where a mutated *Hairless* gene from this strain was transferred into a BALB/c background. The strain was introduced to our institute (National Institutes of Health, at the time of introduction) in 1981. The HRS/J strain was established in 1964 by inbreeding mice obtained by crossing offspring of the hairless mice first found in London [4] with BALB/c mice at the Jackson Laboratory (http://jaxmice.jax.org/strain/000673.html). In addition, the Hos:HR-1 strain was established in 1987 at Hoshino Laboratory Animals Inc. by inbreeding the Skh:HR-1

*(Received 18 February 2013 / Accepted 30 March 2013)*

*Address corresponding: O. Suzuki, Laboratory of Animal Models for Human Diseases, National Institute of Biomedical Innovation, 7–6–8 Saito-Asagi, Ibaraki, Osaka 567-0085, Japan*

outbred strain, which had been established at Temple University by crossing the CBA strain (http://www.hoshino-lab-animals.co.jp/english/products/HR1-en.html) with hairless mice of unknown origin from Sandra Biological Supply. It remains unknown whether HR mice carry the same mutation as other hairless strains, such as HRS/J and Skh:HR-1 (Hos:HR-1), even though the three strains show the same phenotype.

The hairless mutation was first found in a mouse in 1924 [4]. This mutation is an autosomal recessive mutation ($Hr^{hr}$) in the *Hr* gene [11]. Murine *Hr* localizes to the 70-Mb position of mouse chromosome 14, and contains 19 exons [5]. The *hr* mutation is caused by an insertion of the murine leukemia virus into intron 6 [11]. Both HRS/J and Skh:HR-1 (Hos:HR-1) carry this mutation [10]. Homozygous mutants ($Hr^{hr}/Hr^{hr}$) show normal development of the first hair coat (first hair cycle). Starting at 2 weeks of age, they lose their hair coat rapidly and completely due to an abnormal second hair cycle [4, 13]. At weaning (~3 weeks of age), they are completely hairless. In general, females homozygous for $Hr^{hr}$ often fail to nurse their litters due to abnormal lactation (except Hos:HR-1 homozygous females, which show normal lactation; thus, this low nursing activity is thought to depend on the genetic background, not the *Hr* mutation itself). Therefore, most hairless strains have been maintained by mating heterozygous females (normal hair coat) and homozygous males (no hair coat). In this case, pups are a mixture of heterozygous and homozygous mutants. Homozygous mutants cannot be distinguished from heterozygous ones based on appearance alone because they both have coats before 2 weeks of age. Hence, a genotyping method is also needed if younger mice are to be used.

We analyzed the *Hr* gene of the HR strain maintained at our institute to determine if its *Hr* mutation (tentatively called "$Hr^{x}$") is the same as that ($Hr^{hr}$) of other hairless strains (such as HRS/J). In addition, we developed a PCR method to determine the genotypes of pups before the phenotype (hair coat loss) appears (~2 weeks of age) based on the sequence information of HR mice.

## Materials and Methods

*Hairless mice*

At our institute, HR mice (nbio#: nbio003) have been maintained by crossing heterozygous females ($Hr/Hr^{x}$) and homozygous males ($Hr^{x}/Hr^{x}$). Wild-type HR mice (*Hr/Hr*), which had no mutated HR ($Hr^{x}$) alleles, were produced by crossing heterozygous females and males. Hos:HR-1 mice homozygous for hairless genes were purchased from Hoshino Laboratory Animals, Inc. (Bando, Japan) through Japan SLC, Inc. (Hamamatsu, Japan) and used for genotyping tests. All mice were housed under specific pathogen-free conditions with food (CMF, Oriental Yeast Co., Ltd., Tokyo, Japan) and water provided *ad libitum*. All animal experiments were conducted in accordance with the guidelines for animal experiments of the National Institute of Infectious Diseases, Tokyo, Japan, and the National Institute of Biomedical Innovation, Osaka, Japan.

*Genomic PCR*

Hepatic DNA was extracted from homozygous, heterozygous, and wild-type HR mice using an AllPrep DNA/RNA/Protein Extraction Mini Kit (#80004, Qiagen, Hilden, Germany). Primers (Table 1) for PCRs amplifying 15 regions (Fig. 1) in the *Hr* gene were designed based on the *Hr* gene sequence retrieved from the Ensemble database (http://www.ensembl.org). The difference between homozygous ($Hr^{x}/Hr^{x}$) and wild-type (*Hr/Hr*) genomes was determined using multiple PCRs with HotStarTaq (#203443, Qiagen; regions 1, 8–13) or KOD FX neo (KFX-201, TOYOBO, Osaka, Japan; regions 2–7) DNA polymerases. All PCRs were conducted using a Hybaid Sprint thermal cycler (Thermo Scientific, Waltham, MA, USA) in active-tube control mode. Thermal conditions were as follows: for HotStarTaq, 94°C for 15 min (denaturation and enzyme activation), 40 cycles of 94°C for 10 s, 60°C for 10 s, and 72°C for the appropriate amount of time (see Table 2 for elongation time), and then 72°C for 5 min; for KOD FX neo, 95°C for 2 min, 40 cycles of 98.5°C for 10 s and 68°C for the appropriate amount of time (see Table 2 for elongation time), and then 68°C for 5 min. PCR products were separated in agarose gels: for regions 1 and 8–13, 2% E-Gel EX containing SYBR Safe (G4020-02, Life Technologies, Grand Island, NY, USA); for regions 2–7, 0.5% SeaKem LE agarose gels (#50001, Lonza, Basel, Switzerland) with SB buffer (#SB20-1, Faster Better Media LLC, Hunt Valley, MD, USA) and subsequently stained with GelGreen (#41004, Biotium, Inc., Hayward, CA, USA). Stained gels were photographed with a laser scanner (FX Pro, Bio-Rad, Hercules, CA, USA).

**Table 1.** List of primers used in this study

| Name | Sequence (5'- to 3') |
|---|---|
| For genome analysis (Fig. 1) | |
| Int6-F1290 | ACCACCCTGGAATCTTCCGTGAAAAA |
| Int6-R1458 | CATGCTTGCTGTGGAGAGTGCGTGCAT |
| Int6-R539 | CACACACGCAGACAAAACTCACTCGT |
| Int6-R642 | TGGCAGTTTATAGCTGTCTGTCACTCTGG |
| Int6-R850 | TGGGCCACCATGGCCAGATTTAACACA |
| Int6-R979 | CACGTGCATGTGTGGACATGTCTGCCTTA |
| F1843 | CGGCTGTGTGTAGCCTGTGGTCGCATA |
| F1913 | AGCACACAGATGACTGCGCCCAGGAG |
| F193 | TTCCTCCAAGGCCCCAAGGACACACTC |
| F2052 | CTGTTTCTGCCAGGTTGATGCCCGTGT |
| F224 | AGAGCGCTGAGCAGAAAGCGGGAGAAC |
| F2463 | GGGCCTGAGCCTTCCATTGTCACCAGT |
| R1151 | TGGCGTGTGAGCCAGGTCTTTTTCAGC |
| R1873 | CGGCTATGCGACCACAGGCTACACACA |
| R1972 | GGGTCAGGATCAGGGAACAGGCAGCAT |
| R2078 | ACACGGGCATCAACCTGGCAGAAACAG |
| R2433 | TGGCCCCAGGGCTTTCTCTTGGATCTT |
| R3455 | AGGCTGGCTCCCTGGTGGTAGAGCTGA |
| For determining genome sequence in homozygous HR mice (Fig. 2) | |
| mHR-int6-F514 | ACGAGTGAGTTTTGTCTGCGTGT |
| mHR-int6-R806 | CGTAGGTCCTCCTGTTTGCTTGGTCATCA |
| For genotyping (Fig. 3) | |
| mHR-mut-S776 | GGTCTCGCTGGTCCTTGA |
| mHR-int6-S607 | TCTGGAACCAGAGTGACAGACAGCTA |
| mHR-int6-R850 | TGGGCCACCATGGCCAGATTTAACACA |

**Table 2.** DNA polymerase and elongation time for primer sets in Fig. 1

| Primer set in Fig. 1 | DNA polymerase* | Elongation time |
|---|---|---|
| 1 | HotStarTaq | 5 min |
| 2 | KOD FX | 3 min |
| 3 | KOD FX | 6 min |
| 4–7 | KOD FX | 3 min |
| 8, 9 | HotStarTaq | 2 min |
| 10–12 | HotStarTaq | 1 min |
| 13–15 | HotStarTaq | 30 s |

*See Materials and Methods for detailed PCR conditions.

*Determination of DNA sequences flanking the insertion site*

The genomic region containing the insertion mutation site was amplified by PCR from genomic DNA from homozygous HR mice and a set of two primers, mHR-int6-F514 and mHR-int6-R806 (see Table 1), and KOD-FX neo under the following thermal conditions: 95°C for 2 min, 40 cycles of 98.5°C for 10 s and 68°C for 3 min, and then 68°C for 5 min. PCR products, approximately 13 kbp in length, were gel-purified on a 1% agarose gel, and both the 5' and 3' ends were sequenced using an Applied Biosystems 3730 × 1 DNA Analyzer (Life Technologies). The obtained sequence was compared to genome databases at the NCBI using a BLAST search.

*Genotyping PCR*

Primers for genotyping *Hr* alleles were designed according to the sequence information of the alleles (Table 1 for primer sequences; Fig. 3A for primer positions). All three primers were used simultaneously to determine the genotypes of HR and Hos:HR-1 mice. PCRs were conducted using a Hybaid Sprint thermal cycler and HotStarTaq DNA polymerase under the following thermal cycling conditions: 94°C for 15 min, 40 cycles of 94°C for 10 s, 60°C for 10 s, and 72°C for 30 s, and then 72°C for 5 min. PCR products were separated in 2% agarose gels (E-gel EX, G4020-02) and photographed with a laser scanner.

## Results

*PCR analysis of the Hr allele in HR mice*

Analysis of *Hr* alleles in homozygous (H) and wild-type (W) HR mice by means of 15 multiple overlapping PCRs indicated that the $Hr^x$ allele contained an insertion mutation in intron 6 (Fig. 1).